

Supplementary Material for Fast Approximation of Laplace–Beltrami Eigenproblems

Ahmad Nasikun

Christopher Brandt
Delft University of Technology

Klaus Hildebrandt

Introduction

This supplementary material contains additional experimental results concerning the method presented in the submission *Fast Approximation of Laplace–Beltrami Eigenproblems*.

1 Choice of basis functions

In Section 4 of the submission, the construction of the subspace basis is introduced. After sampling, a preliminary matrix $\tilde{U} \in \mathbb{R}^{n \times d}$ in which the i^{th} column represents a locally supported function centered at the sample point v_{s_i} is constructed. The function takes the value one at v_{s_i} , monotonically decreases (in radial direction) in a neighborhood around v_{s_i} , and vanishes outside of the neighborhood. The size of the support of the functions is controlled by a global parameter ρ . We use the cubic polynomial

$$p_\rho(r) = \begin{cases} \frac{2}{\rho^3}r^3 - \frac{3}{\rho^2}r^2 + 1 & \text{for } r \leq \rho \\ 0 & \text{for } r > \rho \end{cases},$$

which satisfies $p_\rho(0) = 1$, $\frac{\partial}{\partial r}p_\rho(0) = 0$, $p_\rho(\rho) = 0$, and $\frac{\partial}{\partial r}p_\rho(\rho) = 0$ for our construction.

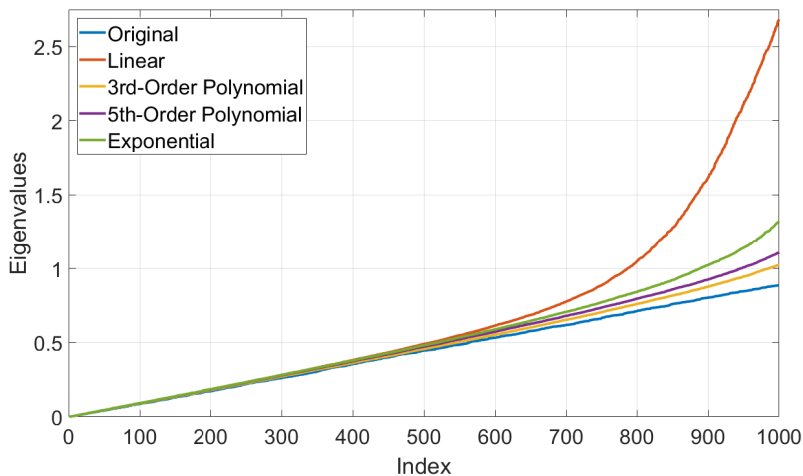


Figure 1: Experimental results that compare the approximate eigenvalues computed using different functions for basis construction to a reference solution are shown.

Of course, other choices of functions are possible. In this section, we describe three alternative choices of functions. Figure 2 shows graphs of the functions for illustration. Figure 1 shows experimental results that compare the resulting approximate eigenvalues to a reference solution.

The first alternative function is the linear polynomial

$$p_\rho^{linear}(r) = \begin{cases} 1 - \frac{r}{\rho} & \text{for } r \leq \rho \\ 0 & \text{for } r > \rho \end{cases},$$

that satisfies $p_\rho(0) = 1$ and $p_\rho(\rho) = 0$. Compared to the cubic polynomial, this polynomial is simpler, but only continuous and not differentiable at ρ .

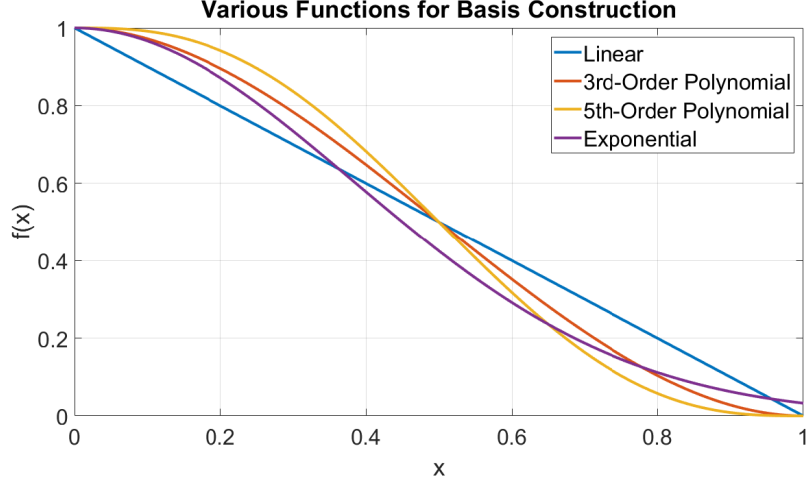


Figure 2: Graphs of the four functions for $\rho = 1$ are shown.

The second alternative is the fifth-order polynomial

$$p_\rho^{fifth}(r) = \begin{cases} -\frac{6}{\rho^5}r^5 + \frac{15}{\rho^4}r^4 - \frac{10}{\rho^3}r^3 + 1 & \text{for } r \leq \rho \\ 0 & \text{for } r > \rho \end{cases},$$

that satisfies $p_\rho(0) = 1$, $\frac{\partial}{\partial r}p_\rho(0) = 0$, $\frac{\partial^2}{\partial r^2}p_\rho(0) = 0$, $p_\rho(\rho) = 0$, $\frac{\partial}{\partial r}p_\rho(\rho) = 0$, and $\frac{\partial^2}{\partial r^2}p_\rho(\rho) = 0$. This polynomial is not just once, but twice differentiable at ρ .

The third alternative is an exponential function

$$p_\rho^{exp}(r) = \begin{cases} e^{-\frac{\log(2)r^2}{0.45^2\rho^2}} & \text{for } r \leq \rho \\ 0 & \text{for } r > \rho \end{cases},$$

that we cut off at ρ .

In our experiments, we compared the approximation error for the eigenvalues we obtain with the different functions and found that the third-order and fifth-order polynomial and the exponential function, produce comparable approximation errors, where the third-order polynomial performs slightly better than the other two. The linear function produced higher errors. An example of results is shown in Figure 1. In this example 1000 approximate eigenvalues that computed in a 1000-dimensional space are shown. Note that in the submission we suggest not to use all 1000 eigenvalues but rather only the first 500.

2 Eigenfunctions and edge flips

To put the approximation results for the Laplace–Beltrami eigenfunctions discussed in Section 5 of the paper into a broader context, we want to add an experiments that explores how the eigenfunctions change when the metric of a surface is slightly changed. For this, we re-meshed the kitten model

by applying a series of edge flips. All vertices are kept in place, but the flips change the metric and hence the discrete Laplace–Beltrami operator. Images of the two meshes are shown in Figure 3. We computed the lowest 500 eigenfunctions of both meshes. To compare them, we looked at the Fourier coefficients, $a_{ik} = \langle \tilde{\Phi}_i, \Phi_k \rangle_{L^2}$, of eigenfunction $\tilde{\Phi}_i$ of the kitten with flipped edges in the eigenbasis $\{\Phi_k\}$ of the kitten before edges are flipped. Plots of the Fourier coefficients of some of the eigenfunctions are shown in Figure 3. We observed that the difference of the eigenfunctions resulting from the edge flips is of similar magnitude as the difference to the approximate eigenfunctions computed with our approximation algorithm as shown in Figure 7 of the paper.

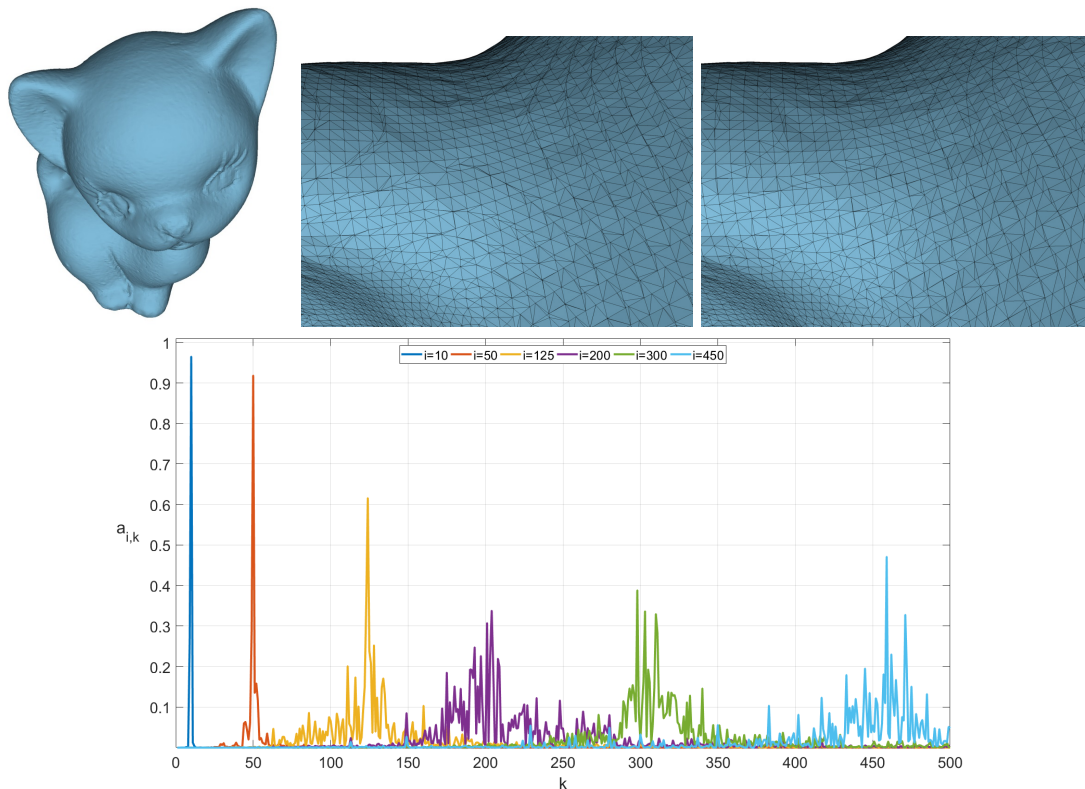


Figure 3: Eigenfunction of the kitten model before and after flipping some edges are compared. The top row show an image of the kitten model and zoom-in images of the mesh before and after some edge flips. The bottom row shows plots of the Fourier coefficients, $a_{ik} = \langle \tilde{\Phi}_i, \Phi_k \rangle_{L^2}$, of eigenfunction $\tilde{\Phi}_i$ of the kitten with flipped edges in the eigenbasis $\{\Phi_k\}$ of the kitten before edges are flipped.

3 Comparison to mesh coarsening

In Section 5 of the submission, the proposed method is compared to a mesh coarsening approach for eigenvalue approximation and Figure 6 (of the submission) shows one example of approximate eigenvalues computed with the proposed method and mesh coarsening. Figure 4 of this supplementary material shows more examples with a comparable setting on different surfaces.

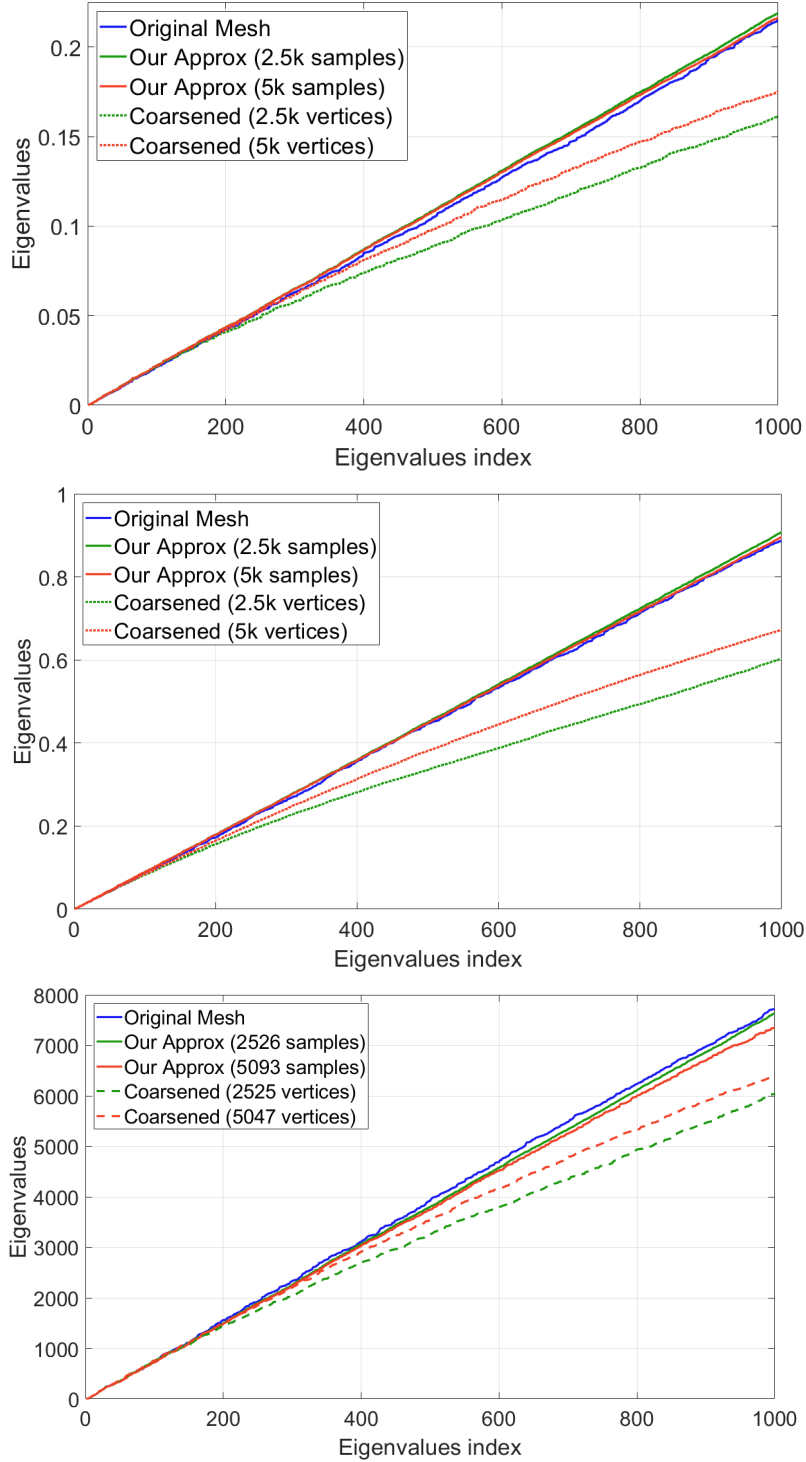


Figure 4: Approximations of the first 1000 eigenvalues of the Laplace–Beltrami operator on the Fertility, the Kitten and the Armadillo mesh are shown. The reference solutions (blue), compute with MATLAB’s sparse eigensolver, is compared with approximations computed with the proposed scheme with 2k (green) and 5k (red) dimensional subspaces and computed from coarsened meshes with 2k (dashed green) and 5k (dashed red) vertices.